Sample Preparation for Study of Space Charge Limited Current

CNF Project Number: 863-00
Principal Investigator(s): John Marohn
User(s): Rachael Cohn, Virginia McGhee

Affiliation(s): Department of Chemistry and Chemical Biology, Cornell University
Primary Source(s) of Research Funding: National Science Foundation
Contact: jam99@cornell.edu, rc784@cornell.edu, vem26@cornell.edu
Website: http://marohn.chem.cornell.edu/
Primary CNF Tools Used: Heidelberg Mask Writer - DWL2000,
ABM Contact Aligner, Odd Hour Evaporator

Abstract:

Scanning probe microscopy is used to study charge injection from a metal to a pi-conjugated system. Unique capabilities of a custom-built electric force microscope will be utilized to reproduce data collected in Ref. [1]. This report discusses substrate preparation conducted at the Cornell NanoScale Science & Technology Facility (CNF) to enable the study space charge limited current.

Summary of Research:

Organic photovoltaics have been steadily growing in both efficiency and functionality [2]. To design and operate organic electronic devices, it is essential to understand how charge is injected from a metal to a pi-conjugated organic system. Typically, there is an assumption that the electric field is uniform between the source and drain gap. However, studies done by Ng, Silveira, and Marohn, show that the electric field varies with both temperature and source-drain voltage [3]. Furthermore, at the injection site, the electric field differs greatly from the bulk, possibly due to the addition of space charge. The previous assumption has an error that propagates through the calculation of electron mobility and concentrations of free charge carriers [1]. To correct for these errors, space charge limited current in an organic photovoltaic film will be studied.

N,N'-diphenyl-N-N'-bis(3-methylphenyl)-(1,1'-biphenyl)-4,4'-diamine (TPD) / polystyrene (PS) films will be spin-coated on quartz substrates. The quartz substrates contain gold interdigitated electrodes prepared at the CNF. The preparation is based on Ref. [1]. The source-drain gap varies in length at 2, 5, 12, 16, and 20 μm, and the channel width varies at 1.5, 2, and 2.5 mm. There are a total of 68 electrodes per substrate and 15 different substrates with the various source-drain gaps and channel widths that can be made on one wafer.

A mask was designed in L-edit and printed using the Heidelberg mask writer. The substrate making process was begun by cleaning quartz wafers with hot piranha, spin coating resist, and exposing the wafer. An exposure matrix using the ABM contact aligner was done to determine the optimal exposure time.

Conclusions and Future Steps:

Users will expose a wafer using the determined exposure time, deposit a 50 Å Cr adhesion layer and 500 Å Au using the odd hour evaporator, lift off to remove excess Au, and dice the wafer to make 1 cm × 1 cm substrates. Once the substrates are completed, users will deposit TPD:PS films and study space charge limited current.

References:

[1] W. R. Silveira and J. A. Marohn, Microscopic view of charge injection in an organic semiconductor, Phys. Rev. Lett., 2004, 93, 116104, URL http://dx.doi.org/10.1103/PhysRevLett.93.116104.

[2] Q. Liu, Y. Jiang, K. Jin, J. Qin, J. Xu, W. Li, J. Xiong, J. Liu, Z. Xiao, K. Sun, S. Yang, X. Zhang, and L. Ding, 18% efficiency organic solar cells, Science Bulletin, 2020, 65, 272–275, URL http://dx.doi.org/10.1016/j.scib.2020.01.001.

[3] T. N. Ng, W. R. Silveira, and J. A. Marohn, Dependence of charge injection on temperature, electric field, and energetic disorder in an organic semiconductor, Phys. Rev. Lett., 2007, 98, 066101, URL http://dx.doi.org/10.1103/PhysRevLett.98.066101.

Nanopatterned Polymer Brushes with Localized Surface Functionalities

CNF Project Number: 1757-09

Principal Investigator(s): Christopher Kemper Ober

User(s): Yuming Huang

Affiliation(s): Department of Materials Science and Engineering, Cornell University
Primary Source(s) of Research Funding: National Science Foundation
Contact: cko3@cornell.edu, yh839@cornell.edu
Website: https://ober.mse.cornell.edu/index.html
Primary CNF Tools Used: E-beam Resist Spinners, JEOL 9500, FilMetrics F50-EXR, Oxford 81 Etcher, Zeiss Ultra SEM, Optical Microscope

Abstract:

It was previously reported that the arrangement of polymer brushes could be organized via an integrated process of electron-beam lithography, surface-initiated synthesis, and post-processing treatments. In this work, the customizability of such polymer nanostructure was further enhanced by chemically functionalizing the chain-ends of these nanopatterned brushes. It was later found that the distribution of these active endpoints was strongly correlated with the polymer chain alignments as characterized by florescence microscopes.

Summary of Research:

Introduction. Polymer brushes are polymer chains with one end covalently anchored to a surface. The development of surface-initiated polymerization enabled the fabrication of polymer brushes with high grafting density. Due to the unusual molecular arrangements and surface attachments, these densely grafted polymer brushes have exhibited unique mechanochemical properties and thus has gained wide interest from the polymer science community [1]. Potential applications of such thin film could be biosensors [2], photovoltaic devices [3], organic electronics [4], and biomimicry surfaces [5].

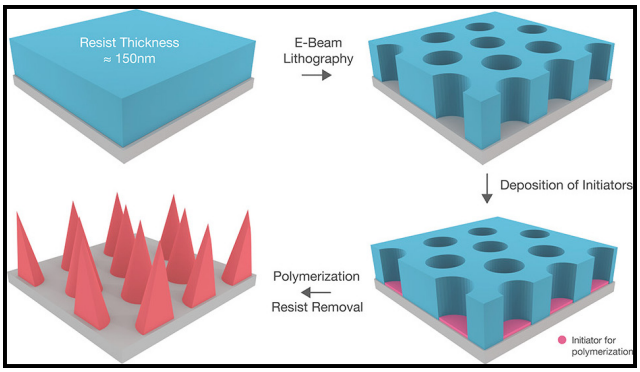

Figure 1: Schematic illustration of the fabrication process of nano-patterned brushes.

Previously we reported a nanopatterning process of making "spiky" nanoarrays of polypeptide rod brushes on silicon substrates, which has resulted in interesting "bridging" morphology governed by the localized chain-chain interactions (Figure 1) [6].

In this work, we further improved the customizability of these nanopatterned polymer brushes by developing end-point modification methods to chemically attach active compounds, such as florescent dyes, to the chain-ends.

Fabrication. The localized growth of polymer brushes was achieved via a sequential fabrication process of area-selective deposition of surface-immobilized initiators and surface-initiated polymerizations.

E-Beam Resist Mask Preparation. E-beam resist was patterned via JEOL 9500, which was later used as the mask for the vapor deposition of aminosilane initiators. Prior to the deposition, the substrate was descummed via the Oxford 81 etcher to remove residual debris in the unmasked area.

Synthesis of the Rod Brushes. The vapor deposition of the silane initiators was carried out in a closed chamber at 1 torr and 70°C for 18 hours. Afterward, the resist mask was removed by sonication in organic solvents. Subsequently, surface-initiated ring-opening

polymerization of poly-b-benzyl-L-glutamate (PBLG), a rod-like polymer, was carried out under continuous vacuum and 105°C for two hours.

End-Point Functionalization. 5 mg of rhodamine B isothiocyanate was dissolved in 2 ml of an hydrous dimethylformamide (DMF) together with a piece of PBLG brush sample. Then 0.8 ml of triethylamine was added to the solution. The reaction was allowed to proceed for 48 hours and the substrate was taken out, rinsed and sonicated in DMF for one minute and dried with nitrogen gas.

Characterization and Results. The thickness of the thin film was measured by FilMetrics F50-EXR. The patterned e-beam resist (Figure 2) and the patterned PBLG brushes (Figure 3) were characterized using Zeiss Ultra Scanning Electron Microscopy (SEM) and Veeco Icon Atomic Force Microscope (AFM) for topological analysis. The florescence behavior of the modified brushes was characterized using Zeiss LSM 710 confocal microscope (Figure 4).

Conclusions and Future Steps:

In addition to nanolithography and post-processing treatment, we have demonstrated that polymer nanostructures can be further customized by chemical modification of the chain-ends. The distribution and molecular arrangements of these active chain-ends can be examined by the behavior of the attached florescence molecules. In the near future, we plan to explore the possibility of functionalizing these nanostructures with bio-active compounds for biomimicry surface and modeling study. We also plan to introduce mixed rod-coil brushes in the same system for binary and stimuli-responsive surface functionalities.

References:

[1] W. L. Chen, M. Menzel, T. Watanabe, O. Prucker, J. Ruhe, and C. K. Ober, "Reduced Lateral Confinement and Its Effect on Stability in Patterned Strong Polyelectrolyte Brushes," Langmuir, vol. 33, no. 13, pp. 3296-3303, 2017, doi: 10.1021/acs.langmuir.7b00165.

[2] M. Welch, A. Rastogi, and C. Ober, "Polymer brushes for electrochemical biosensors," Soft Matter, vol. 7, pp. 297-302, 2011, doi: 10.1039/c0sm00035c.

[3] S. Saha and G. L. Baker, "Surface-tethered conjugated polymers created via the grafting-from approach," J Appl Polym Sci, vol. 132, no. 4, p. n/a-n/a, 2015, doi: 10.1002/app.41363.

[4] N. Doubina, et al., "Surface-initiated synthesis of poly(3-methylthiophene) from indium tin oxide and its electrochemical properties," Langmuir, vol. 28, pp. 1900-8, 2012, doi: 10.1021/la204117u.

[5] Z. Zhou, P. Yu, H. M. Geller, and C. K. Ober, "Biomimetic polymer brushes containing tethered acetylcholine analogs for protein and hippocampal neuronal cell patterning," Biomacromolecules, vol. 14, pp. 529-37, 2013, doi: 10.1021/bm301785b.

[6] Y. Huang, H. Tran, and C. K. Ober, "High-Resolution Nanopatterning of Free-Standing, Self-Supported Helical Polypeptide Rod Brushes via Electron Beam Lithography," ACS Macro Lett, vol. 10, no. 6, pp. 755-759, 2021, doi: 10.1021/acsmacrolett.1c00187.

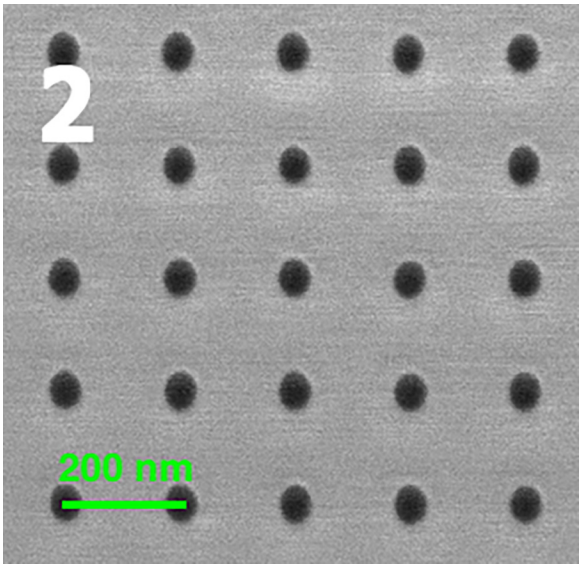

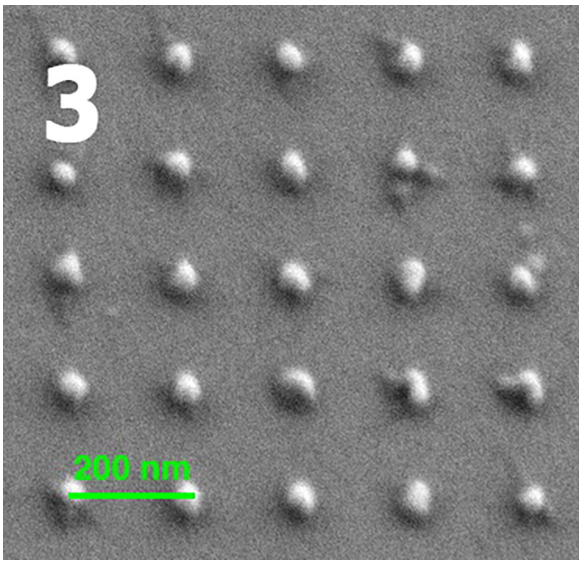

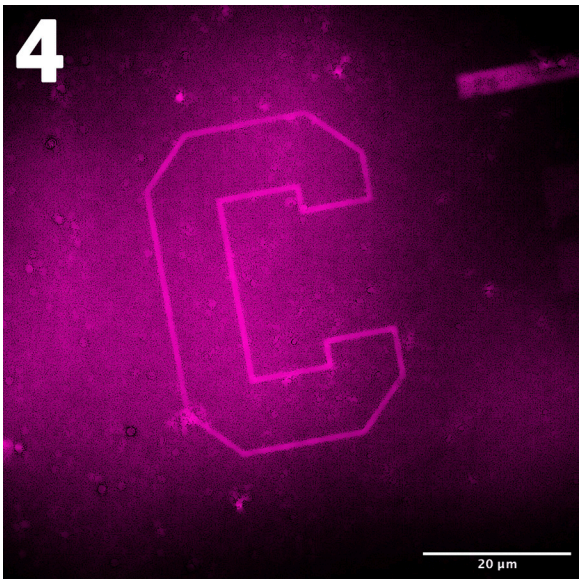

Figure 2, top: SEM of the patterned e-beam resist. Figure 3, middle: SEM of the patterned PBLG rod brushes. Figure 4, bottom: Florescence image of the rhodamine B functionalized patterned brushes.

Chemically Amplified Photoresists with Precise Molecular Structure

CNF Project Number: 1757-09

Principal Investigator(s): Christopher Kemper Ober

User(s): Florian Hermann Ulrich Kaefer

Affiliation(s): Department of Material Science and Engineering, Cornell University

Primary Source(s) of Research Funding: Intel

Contact: cko3@cornell.edu, hk28@cornell.edu

Website: https://ober.mse.cornell.edu/

Primary CNF Tools Used: ASML 300C DUV Stepper, AFM Bruker Icon, JEOL 6300 E-Beam, Woollam RC2, Zeiss Ultra SEM, YES HMDS Prime Oven

Abstract:

In most synthetic copolymers, monomer units are distributed randomly along the polymer chain. In sequence-controlled polymers such as peptides and peptoids, however, monomers are arranged in a specific, application-optimized order. Polypeptoids are thus attractive as a new category of photoresists for EUV lithography, as full control over the placement of individual functional groups yields in tunable properties with extremely low chemical, structural, and molar mass variability [1-3]. This report demonstrates the potential use of peptoids CAR resist using an electron-beam and deep-UV (DUV) lithography obtaining 36 nm line pattern.

Introduction:

Polymeric resists are typically based on random copolymers. These polymers are polydisperse and relatively large in size, with molar masses ranging from 5,000-15,000 g/mol [1]. Characteristics such as these can have a negative impact on resist performance, and therefore it is necessary to explore other architectures for new resist platforms. As a result, there has been research on using molecular glasses as photoresists due to their defined, repeatable structure, and low molecular weight compared to conventional polymeric photoresists. Like molecular glass, peptoids can be synthesized with a controlled sequence and chain length. Due to these properties, it is hypothesized that using peptoids as photoresist material may be the next promising path towards smaller feature sizes.

The goal of this project is to investigate and optimize the composition and sequence of the synthesized short peptoids to obtain resist with high resolution and good processibility, as the precise sequence of moieties is key to tuning the nano- and macro-scale characteristics of the resulting resists.

Results:

Peptoids with 10 repeat units were synthesized using a solid phase peptoid synthesis approach [3]. After activating the resin with bromoacetic acid for 30 min the first amine solution was added and the reaction was completed after 60 min. These steps were repeated until a peptoid with a total length of ten amines with a defined sequence was obtained, see Figure 1. Subsequently, the peptoid was cleaved from the resin under mild acetic conditions, purified and dried. Di-tert butyl decarbonate was used to protect the hydroxy groups to introduce solubility switching groups.

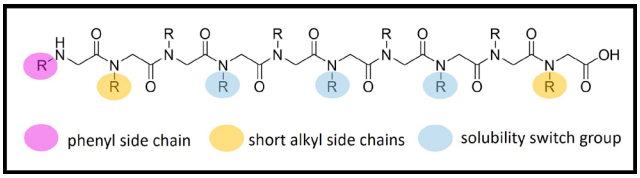

Figure 1: Peptoid 10mers used as positive tone chemically amplified resist (CAR).

The synthesized peptoids were characterized using matrix assisted laser desorption ionization (MALDI) time of flight (TOF) mass spectrometry, and differential-scanning calorimetry (DSC).

Resists with different sequences, composition, and hydrophobic side groups, were dissolved and spin coated on 4-inch silicon wafers. The resist film thickness was measured using a Woollam RC2 ellipsometer. The resist films were exposed using deep-UV (DUV) (ASML 300C stepper) and electron-beam (JEOL 6300). Sequence, composition, and the choice of hydrophobic side groups led to significantly changes in the solubility and performance.

The obtained patterns were characterized using scanning-electron microscopy (SEM) and atomic force microscopy (AFM Bruker Icon), see Figure 2. The micrographs of 24 nm-line pattern are demonstrating the potential of peptoids as new class of resists while the sequence, composition and total length are adjustable and are changing and affecting the lithographical performance. However, further research must be carried out to further improve the lithographical performance and demonstrate the potential of peptoids as a new generation of EUV resists.

Conclusions and Future Steps:

Sequence controlled peptoids were synthesized and successfully used as positive tone photoresist using the DUV and electron beam lithography. The obtained line patterns were characterized via SEM and atomic force microscopy, and proved the potential of peptoids as resists for electron and EUV lithography. However, further research on these new class of resists materials is required to optimize the properties of the resist as well as their performance.

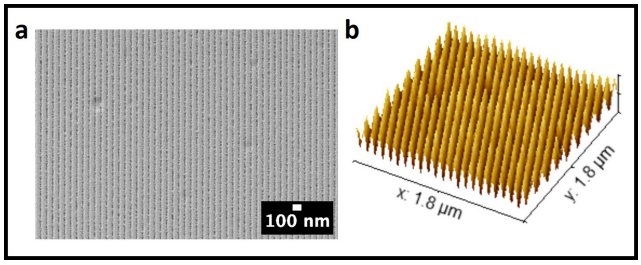

Figure 2: Line pattern by e-beam (a) SEM of line pattern 36 nm, (b) AFM 3D height profile.

References:

[1] Patterson, K.; Yamachika, M.; Hung, R.; Brodsky, C.; Yamada, S.; Somervell, M.; Osborn, B.; Hall, D.; Dukovic, G.; Byers, J.; Conley, W.; Willson, C. G., Polymers for 157-nm photoresist applications: a progress report. SPIE: 2000; Vol. 3999.

[2] Gangloff, N.; Ulbricht, J.; Lorson, T.; Schlaad, H.; Luxenhofer, R., Peptoids and Polypeptoids at the Frontier of Supra- and Macromolecular Engineering. Chemical Reviews 2016, 116 (4), 1753-1802.

[3] Culf, A. S.; Ouellette, R. J., Solid-phase synthesis of N-substituted glycine oligomers (alpha-peptoids) and derivatives. Molecules (Basel, Switzerland) 2010, 15 (8), 5282-5335.

Identifying the Occurrence and Sources of Per- and Polyfluoroalkyl Substances in Photolithography Wastewater

CNF Project Number: 2938-21

Principal Investigator(s): Damian Helbling, Christopher Kemper Ober

User(s): Paige Jacob

Affiliation(s): Civil and Environmental Engineering, Cornell University

Primary Source(s) of Research Funding: Semiconductor Research Corporation, National Science Foundation

Contact: deh262@cornell.edu, cko3@cornell.edu, pv7@cornell.edu
Website: https://helbling.research.engineering.cornell.edu/

Primary CNF Tools Used: DISCO Dicing Saw, Jelight 144AX UVO-Cleaner, FilMetrics F40

Abstract:

Per- and polyfluoroalkyl substances (PFASs) are contaminants of emerging concern to environmental and human health [1]. PFASs are present in chemical mixtures used during photolithography [2] and might undergo transformation reactions during the steps of photolithography. We acquired five photolithography materials and characterized the occurrence of PFASs in the native materials. We performed photolithography and collected the resulting wastewater samples to evaluate the chemical transformations. The goal of the project is to elucidate the sources of and mechanisms by which PFASs are introduced or generated during photolithography.

Summary of Research:

The occurrence of PFASs in wastewater and fresh water has emerged as a challenge for engineers [1]. A major obstacle for water quality managers and policy makers is that there are thousands of known PFASs, and countless others that may arise from transformation reactions during industrial processing, environmental transport, or water and wastewater treatment [3]. A variety of PFASs are used in photolithography and a recent study demonstrated that photolithography wastewater contains known and previously unknown PFASs [4]. Although it is known that perfluorobutane sulfonate (PFBS) is a widely used constituent of photoacid generators (PAGs) [2], the sources of nearly all of the other PFASs in photolithography wastewater remain unknown.

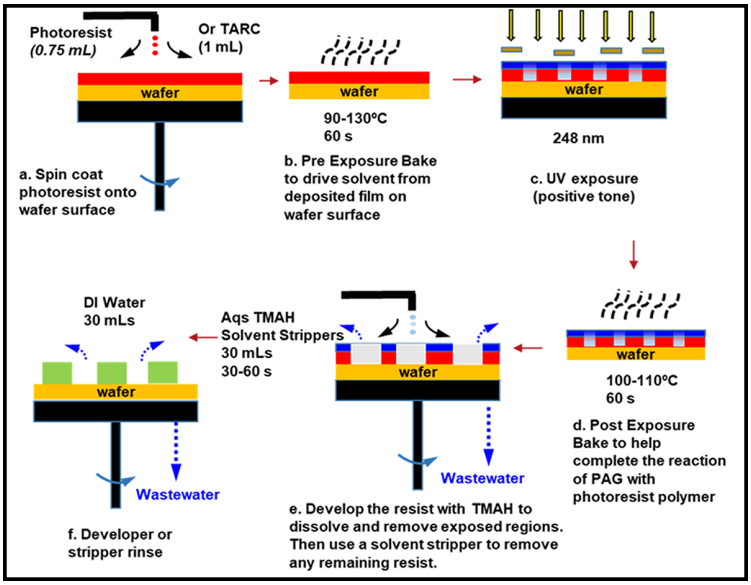

Figure 1: Process diagram of the photolithography workflow conducted at the CNF for each of the five native materials. In this figure, "DI water" = deionized water, and "TMAH" = tetramethylammonium hydroxide.

The complex materials are also subject to transformation reactions induced by the chemical conditions of photolithography. Photolithography requires the application of the photoresist through spin-coating followed by a soft bake, 248 nm exposure, a hard bake, development, and stripping [5]. These steps expose the materials to UV radiation and highly basic conditions. We hypothesize that many PFASs measured in photolithography wastewater are transformation products formed during photolithography.

The goal of the project is to elucidate the sources of and mechanisms by which PFASs are introduced or generated during photolithography. We also aim to study transformation pathways, as improved understanding of transformation pathways will lead to better predictions

Chemical	Measured TOF (g/L)
Photoresist A	1.65±0.14
Photoresist B	0.36±0.03
Photoresist C	1.31±0.04
TARC A	18.1±0.35
TARC B	4.62±0.08

Figure 2: Total organic fluorine measurements of each of the native photolithography mixtures.

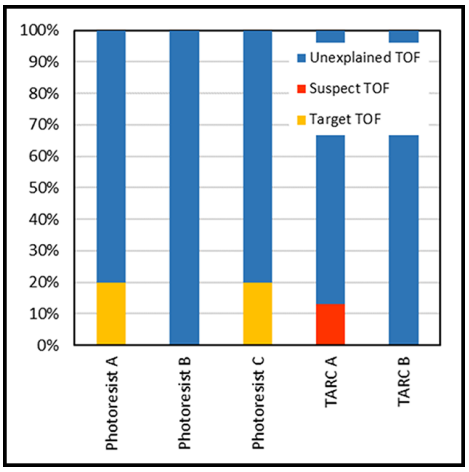

Figure 3: Percentage of total organic fluorine measurements that are accounted for by target or suspect PFASs in the native materials.

of how chemicals transform and inform the development of new photolithography chemicals.

First, we acquired five industrially relevant photolithography materials consisting of three photoresists (Photoresists A, B, and C) and two top antireflective coatings (TARCs A and B). We identified and quantified the PFASs in the materials with multiple analytical techniques, including two high resolution mass spectrometry (HRMS) analyses and a combustion ion chromatography (CIC) analysis. The HRMS analyses consisted of a target screening, where authentic standards of 35 target PFASs and isotope-labelled internal standards were used to quantify PFASs in the materials, and a suspect screening, where HRMS data was mined to gather qualitative information on a list of 171 PFASs that were previously identified in photolithography wastewater samples. The CIC analysis combusts all fluorinated compounds directly into hydrogen fluoride (HF) and the fluoride is then measured with IC to quantify the total organic fluorine (TOF) in the sample [3].

Next, at the CNF we manually performed the steps of photolithography and collected the wastewater from a single material after development and stripping to identify which step may be inducing transformations (Figure 1). We also performed photolithography on clean wafers and collected wastewater samples to characterize the background contamination of PFAS within the CNF and to determine which PFASs are derived from the native materials.

Then we performed target and suspect screenings on the wastewater samples to identify the PFASs present post-photolithography. In addition to collecting wastewater samples, the DISCO dicing saw to was used to cut wafers into pieces that would fit inside the combustion unit to measure the TOF of the wafer after each step of photolithography. Lastly, the FilMetrics F40 was used for thickness measurements of the wafers after each step of photolithography. These measurements will allow us to calculate a mass balance of the native materials on the wafer throughout photolithography.

Conclusions and Future Steps:

The results of the target screening of the five materials revealed the presence of only one target PFAS in two of the materials. Photoresists A and C contained PFBS, which is probably used as the PAG anion in these materials, at concentrations of 331 and 268 mg L-1, respectively. The suspect screening results revealed that suspect PFASs were only identified in TARC A. Photoresist B and TARC B did not contain any target or suspect PFASs.

Next, the samples were analyzed by means of CIC for TOF. The TOF measurements of each photolithography material were in the g L-1 range (Figure 2). We also found that TARCs have higher concentrations of TOF, sometimes an order of magnitude higher than photoresists. These measurements display a gap between the TOF accounted for with target and suspect compounds and the total TOF in the materials, leaving a fraction of the TOF unexplained (Figure 3).

After photolithography, we observed that PFBS was still the main target PFAS identified in post- photolithography wastewater samples and was present in the µg L-1 range. We identified a limited number of other target and suspect PFASs in the wastewater samples. We will next analyze the HRMS acquisitions of the wastewater for unexpected PFASs and measure the TOF of the wastewater and wafer samples.

After identifying the PFASs generated during photolithography, we aim to identify transformation reaction pathways for the fluorinated constituents in native materials to identify reactions occurring at each step and link parent chemicals to the products found in the wastewater from that step. Additionally, we are currently in the process of obtaining a 193 nm exposure tool and temporarily installing it within the CNF to perform the same workflow at 193 nm exposures.

References:

[1] Z. Wang, et al.; 10.1021/acs.est.6b04806.

[2] C. K. Ober, et al.; 10.1117/1.JMM.21.1.010901.

[3] C. A. McDonough, et al.; 10.1016/j.coesh.2018.08.005 (4) P. Jacob, et al.; 10.1021/acs.est.0c06690.

[4] D. Bratton, et al.; 10.1002/pat.662.